ACS OMEGA

http://pubs.acs.org/journal/acsodf

Article

Nitrogenated Graphene Oxide-Decorated Metal Sulfides for Better Antifouling and Dye Removal

Lavanya Chandra, Kusuma Jagadish, Vinothkumar Karthikeyarajan, Mohammed Jalalah, Mabkhoot Alsaiari, Farid A. Harraz,* and R Geetha Balakrishna*

Cite This: *ACS Omega* 2022, 7, 9674–9683

Read Online

ACCESS | Metrics & More | Article Recommendations | Supporting Information

ABSTRACT: Nitrogenated graphene oxide-decorated copper sulfide nanocomposites (Cu_xS-NrGO, where x = 1 and 2) are designed to be incorporated in polysulfone (PSF) membranes for effective fouling resistance of PSF membranes and their dye removal capacity. The developed membranes possess more hydrophilicity and an enhancement in pure water flux (PWF). Also, the highest bovine serum albumin (BSA) rejection of 89% was observed when compared to membranes with pristine PSF (5 L/m^2 h PWF and 88% BSA rejection) and CuS-incorporated PSF membranes (14 L/m^2 h PWF and 83% BSA rejection) because of N doping and enhanced permeability. It is also found that the Cu_xS-NrGO-incorporated PSF membranes exhibited a significantly higher fouling resistance, a larger permeate flux recovery ratio (FRR) of nearly 82%, and a congo red dye rejection of 93%. Cu_xS-NrGO nanoparticles thus demonstrate the potential efficacy of enhancing the hydrophilicity, leading to a better flux, dye removal capacity, and antifouling capacity with a very high FRR value of 82% because of a strong interaction between the N-active sites of the NrGO, Cu_xS, and polysulfone matrix, and negligible leaching of nanoparticles is observed.

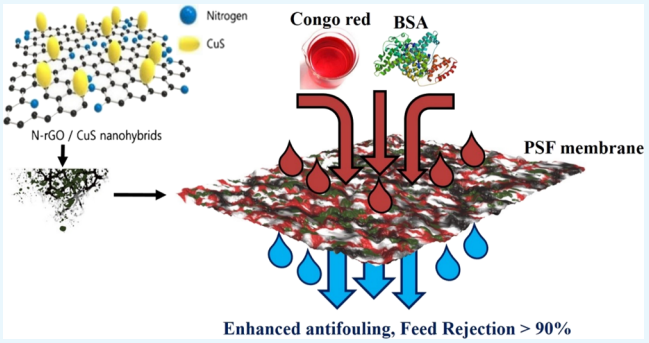

1. INTRODUCTION

Polymeric membranes have attracted significant attention in ultrafiltration membrane processes due to their various advantages such as excellent film-forming properties, strong thermal and chemical stability, and outstanding resistance in acidic and alkaline conditions.[1] In addition, these membranes have superior separation efficiency and easy scale-up and maintenance. However, the hydrophobic property of these membranes leads to severe membrane fouling causing a decline in water flux and deterioration of membrane quality.[2,3] The demand for high energy in using these fouled membranes, costly cleanup of fouled membranes, and repeated replacement of membranes[4,5] restrict their practical application in various fields. Thus, the modification of these membranes is highly recommended. Fabrication of composite or mixed matrix membranes (MMMs) through both ex situ and in situ incorporation of various inorganic nanoparticles[2,5] has to some extent provided relief to fouling difficulties.

On the other hand, although polysulfone is one of the most extensively used polymeric materials to fabricate membranes owing to its excellent environmental endurance, chemical, thermal, and mechanical stability, and superior film-forming properties,[6] its hydrophobic nature is undesirable and leads to quick fouling. Modification of such membranes and uplifting of hydrophilicity of these membranes can resist fouling. Modification techniques such as blending with hydrophilic additives,[7,2] graft polymerization,[4] ultraviolet irradiation,[4] and surface modification[8] have led to some enhanced improvement in the antifouling property of membranes. However, among the mentioned techniques, blending with hydrophilic inorganic nanoparticles is proven to be an excellent approach in enhancing the permeability and antifouling ability of membranes.[9]

Graphene oxide (GO) synthesized from the modified Hummers' method is shown as a potentially better candidate to be used as a hydrophilic additive[10,11] in membranes for better permeability,[11] antifouling property,[12] and antibacterial activity[5] owing to its low cost, ease of scale-up, functional group abundance, high surface area, and easy functionalization of the surface.[11,12] Doping of heteroatoms (viz., B, N, and S) is a potent method for modifying graphene oxide to improve the thermal and electrical properties and to enhance the densities of free charge carriers. Also, the doping of heteroatoms

Received: December 18, 2021
Accepted: February 23, 2022
Published: March 8, 2022

https://doi.org/10.1021/acsomega.1c07140
ACS Omega 2022, 7, 9674–9683

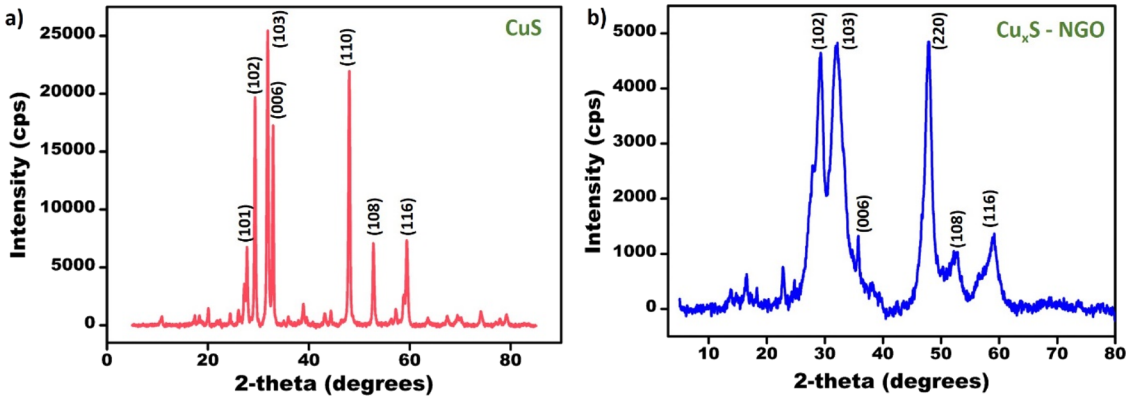

Figure 1. XRD patterns of (a) CuS and (b) Cu$_x$S-NrGO nanoparticles.

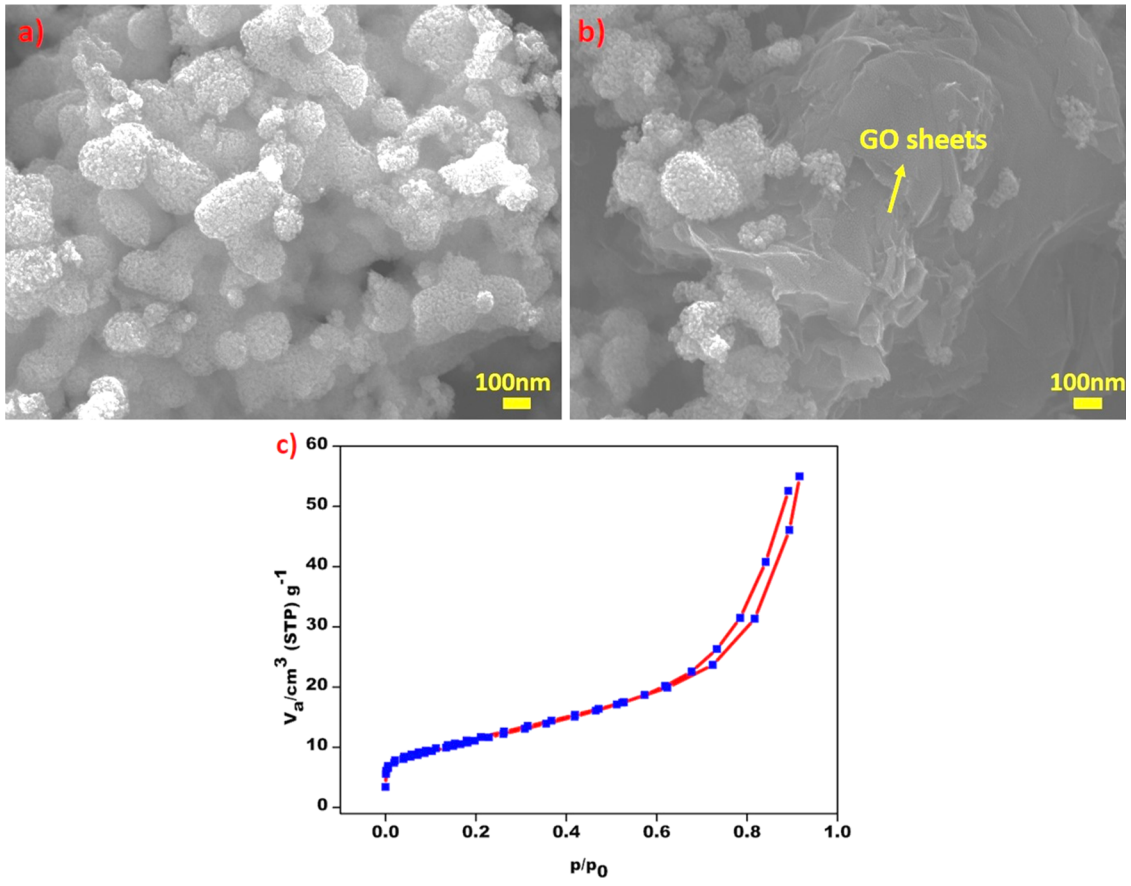

Figure 2. (a,b) FESEM images of Cu$_x$S-NrGO nanoparticles and (c) adsorption/desorption isotherms of Cu$_x$S-NrGO nanoparticles.

changes the elemental composition of GO, which in turn changes the intrinsic properties of GO.[13] Among several dopants mentioned above, nitrogen's ionic radius is almost comparable to that of carbon, which makes nitrogen an ideal and promising candidate to be doped into GO, and few other applications of N-doped GO can be found.[14−16] A strong interaction between the π electrons of GO and the lone-pair electrons of nitrogen dominantly overcomes the agglomeration leading to better dispersion in suitable organic solvents. Doping of GO with nitrogen helps in increasing the interlayer spacing between GO sheets, which in turn increases the surface area, reduces agglomeration, and enhances the conjugated structure; rGO sheets otherwise tend to agglomerate (when there is no heteroatom doping) because of their strong $\pi-\pi$ interactions, which in turn reduces the specific surface area. Additionally, N-doped GO contributes to more hydrophilicity because of a higher number of N-active sites.[17] Thus, N-doped rGO has attracted much emphasis during recent years because of its importance in various applications such as catalysis,[16] water purification,[14] sensors,[18] and energy storage and conversion.[14,16,18,19]

N-doped GO supported on metal nanoparticles presents outstanding stability, catalytic activity, and electronic properties because the N doping of GO provides strong interaction with the metal nanoparticles, which helps in generating more active sites and electrical conductivity.[20] The N-active sites increase the affinity toward water molecules, which makes the N-doped GO-supported metal nanoparticles more hydro-

https://doi.org/10.1021/acsomega.1c07140
ACS Omega 2022, 7, 9674−9683

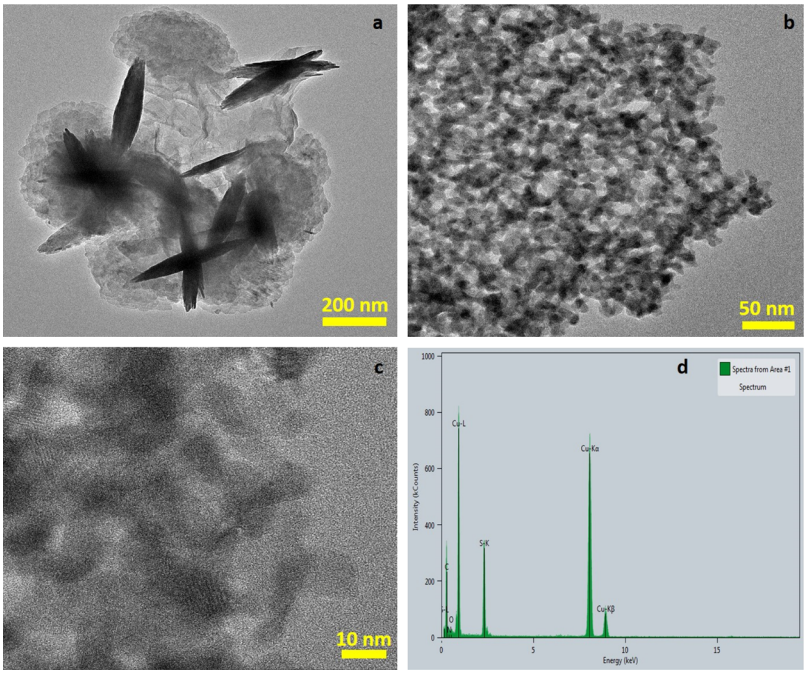

Figure 3. (a,b) TEM images of Cu_xS-NrGO at different magnifications, (c) HRTEM image, and (d) EDX spectrum of Cu_xS-NrGO nanoparticles.

philic.[21] Recently, copper sulfide nanoparticles decorated on functionalized GO nanosheets displayed exceptional betterment in their hydrophilicity, permeability, surface charge, and antifouling ability.[22] Due to their cost-effectiveness, they have been widely used in various industries. They are also used in the degradation of various organic pollutants and in water purification.[23] An attempt to nitrogenate GO (to increase the hydrophilicity and reduce agglomeration) and form Cu_xS-NrGO via in situ synthesis (to create more active sites and to reduce agglomeration) was carried out for the first time, and it was used as a hydrophilic additive to blend with PSF. The synthesized particles and their interaction with membranes were evaluated for structural confirmation, morphology, and hydrophilicity. The performance of the membranes was studied in terms of the pure water flux (PWF), dye removal capacity, and antifouling property. The obtained results are compared with those of PSF membranes incorporated with CuS and CuS-rGO (no nitrogenation) nanoparticles. The positive effect of nitrogenation in such application (done for the first time) is discussed. Strong coordination between these hydrophilic particles (as shown in Figure 7) with membranes not only avoids leaching of these particles but renders a remarkable antifouling property with retention of the rejection ability and enhancement of the PWF.

2. RESULTS AND DISCUSSION

2.1. Material Characterization. Nitrogenated rGO−Cu_xS nanohybrid formation and phases were confirmed using p-XRD as shown in Figure 1. The XRD pattern of CuS nanoparticles is shown in Figure 1a depicting 2θ values of 28.7, 29.3, 31.8, 32.9, 48.0, 52.7, and 59.3° corresponding to the planes (101), (102), (103), (006), (110), (108), and (116), respectively, of covellite, which matches well with the reference pattern (JCPDS no. 06-0464). Figure 1b presents the XRD pattern of synthesized Cu_xS-NrGO nanoparticles (copper exists in both +1 and +2 oxidation states as confirmed from XPS analysis). The XRD diffraction peaks of Cu_xS-NrGO correspond to both hexagonal CuS (ICDD no. 06-0464) and cubic Cu_2S (ICDD no. 053-522). The peaks corresponding to the (220) plane are due to cubic Cu_2S, whereas reflections corresponding to the (102), (103), (006), (108), and (116) planes are due to hexagonal CuS.[24] There is no diffraction peak corresponding to GO, which could be due to its low diffraction intensity. In order to understand it better, the XRD spectrum of CuS-rGO (50:50) is also given in the Supporting Information (Figure S1).

Figure 2a,b shows the surface properties of Cu_xS-NrGO hybrid powder analyzed by FESEM. Surface images suggest highly porous nanostructures (surface area of ∼41 $m^2\ g^{-1}$) of Cu_xS distributed over graphene oxide sheets. Doping of N heteroatoms has caused the Cu_xS to be highly mesoporous (pore diameter of 8.13 nm). BET adsorption/desorption isotherms in Figure 2c suggest a type IV reversible isotherm and mesoporosity with a surface area of 41.89 $m^2\ g^{-1}$; however, the observed surface area of CuS-rGO was found to be lower (∼17.55 $m^2\ g^{-1}$) (Figure S2c) with a pore diameter of 10.22 nm. The lower surface area in the case of CuS-rGO is because of its agglomeration tendency due to strong $\pi-\pi$ interaction. FESEM images of CuS-rGO nanoparticles are given in the SI (Figure S2) where the CuS nanoflowers are scattered on rGO sheets suggesting the roughly uniform distribution of CuS-rGO nanoparticles.

Figure 3a,b shows the transmission electron microscopic images of the Cu_xS-NrGO nanohybrid at different magnifications. The average particle size of Cu_xS nanoparticles is around 12−15 nm, which are well wrapped in graphene oxide sheets (Figure 3a) with clear lattice fringes for GO sheets and Cu_xS nanoparticles (Figure 3c), which confirms the strong interaction between the GO sheets and Cu_xS nanoparticles as shown in Figure 1, and Cu_xS cannot be found outside the GO sheets. Also, no agglomeration was observed in Cu_xS-NGO because of N doping and rich active sites when compared to CuS-rGO nanoparticles. The elemental analysis as shown in the EDX spectrum of Figure 3d confirms the

https://doi.org/10.1021/acsomega.1c07140
ACS Omega 2022, 7, 9674−9683

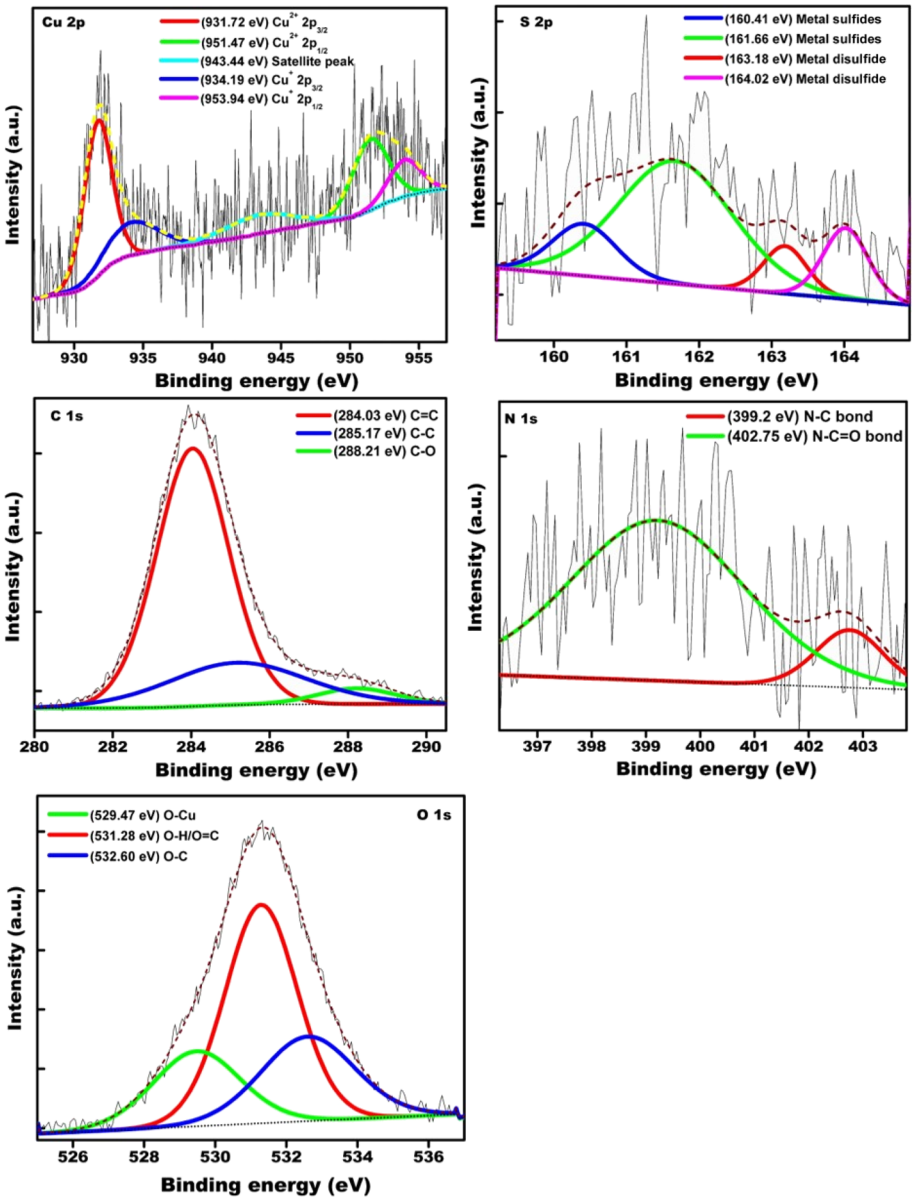

Figure 4. XPS spectra of Cu_xS-NrGO nanoparticles.

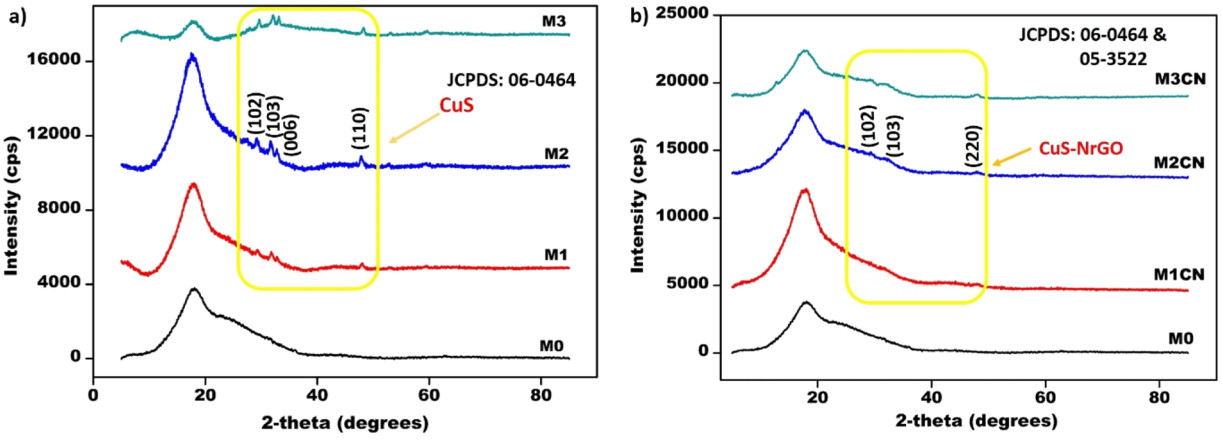

Figure 5. XRD patterns of (a) PSF-CuS membranes and (b) PSF-Cu_xS-NrGO membranes.

presence of N, Cu, S, C, and O, which affirms the successful formation of Cu_xS-NrGO. TEM images and the EDX spectrum of CuS-rGO nanoparticles are given in the SI (Figures S3 and S4) where the flower-like CuS samples are wrapped in rGO

https://doi.org/10.1021/acsomega.1c07140
ACS Omega 2022, 7, 9674−9683

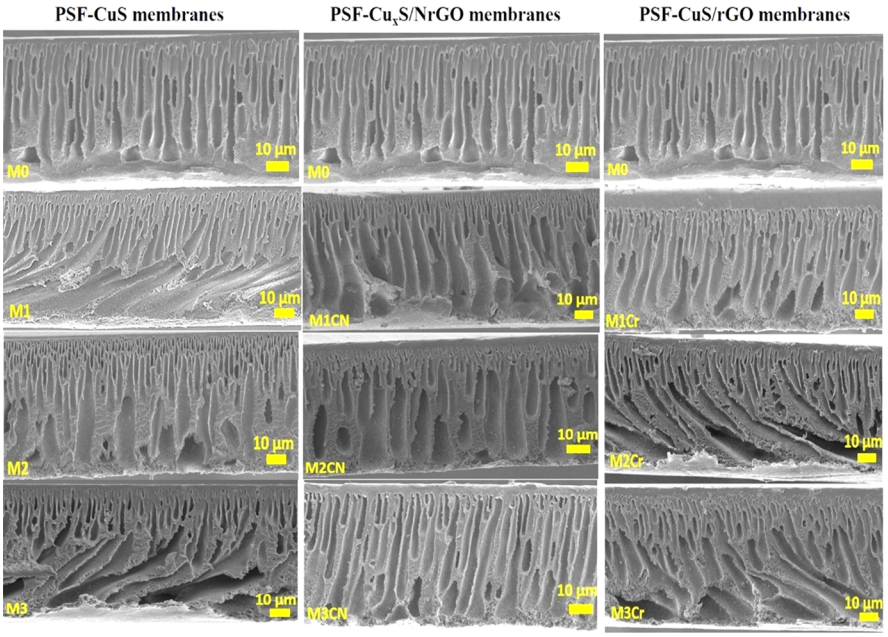

Figure 6. Cross-sectional FESEM images of the pristine PSF membrane and its composites with CuS, Cu_xS-NrGO, and CuS-rGO nanoparticles.

sheets and the clear lattice fringes for graphene oxide sheets are seen.

Elemental analysis of the nanohybrid is shown in Figure 4. The high-resolution spectrum of Cu 2p in Figure 4 is deconvoluted into five individual peaks. The peaks at binding energy values of 931.72 and 951.47 eV correspond to the $2p_{3/2}$ and $2p_{1/2}$ split orbitals of the Cu^{2+} ion, and those at 934.19 and 953.94 eV correspond to $2p_{3/2}$ and $2p_{1/2}$ split orbitals of the Cu^{+} ion. The peak at 943.44 eV is the satellite peak of Cu $2p_{3/2}$ photoelectrons. Further, the S 2p spectrum is deconvoluted into four peaks at 160.41 and 161.66 eV and 163.18 and 164.02 eV for metal sulfide bonds and metal disulfide bonds, respectively. The C 1s spectrum is deconvoluted into three peaks at 284.03, 285.17, and 288.21 eV corresponding to C═C, C−C, and C−O, respectively. The N 1s high-resolution XPS spectrum in Figure 4 shows two peaks at 399.2 and 402.75 eV corresponding to N−C and N−C═O bonding, respectively.[18] The high-resolution XPS spectrum of O 1s is deconvoluted into three individual peaks with binding energy values of 529.47, 531.28, and 532.60 eV corresponding to O−Cu bonding (might be from the CuO layer formed on the material surface), O−H/O═C, and O−C bonds present in the graphene oxide species, respectively.

2.2. Membrane Characterization. *2.2.1. XRD Patterns of Modified PSF Nanocomposite Membranes.* Figure 5 displays the XRD patterns of PSF-CuS membranes and PSF-Cu_xS-NrGO membranes. The successful incorporation of CuS (Figure 5a) and Cu_xS-NrGO (Figure 5b) nanoparticles was confirmed by the presence of intense peaks between 25 and 55° as marked, among which the 1.5 wt % PSF-CuS and 1.5 wt % Cu_xS-NrGO membranes showed more intense peaks because of the presence of larger amounts of nanoparticles in the PSF nanocomposite membranes. The XRD spectrum of the CuS-rGO-incorporated PSF membrane is given in the SI (Figure S5). Peaks appear to be broadened and less intense in Cu_xS-NrGO membranes due to the incorporation of wider spaced NrGO films along with CuS. These results are similar to earlier reports observed by Boytsov et al.[25] and AlShammari et al.[26]

2.2.2. FESEM Images of PSF Nanocomposite Membranes. Figure 6 depicts the cross-sectional FESEM images of prepared composite membranes. Finger-like projections with a denser top layer and macrovoids at the bottom were observed in all the membranes due to the asymmetric nature of membranes. The Cu_xS-NrGO (M1CN−M3CN) composite membranes show wider and elongated finger-like structures with undisturbed channels as compared to the pristine PSF (M0) membrane, PSF-CuS (M1−M3), and PSF-CuS-rGO (M1Cr−M3Cr) membranes. The higher hydrophilic nature of the Cu_xS-NrGO nanohybrids controls the exchange of the solvent and the nonsolvent during the phase inversion process, thus leading to a higher porosity and more elongated pores with undisturbed channels in the membranes. In the case of PSF-CuS-rGO membranes, a thicker skin layer with disturbed channels was observed. However, when the concentration of the nanoparticle loading was increased from 0.5 to 1.5 wt % (with a 0.5 wt % increment each time), the thickness of the skin layer increased due to high viscosity of the casting solution with slightly spongy walls observed at the bottom. The optimum concentration in the case of PSF-CuS and CuS-rGO membranes was found to be 1 wt % nanoparticle loading, whereas it was found to be 1.5 wt % in the case of Cu_xS-NrGO membranes.

2.2.3. Contact Angle Values of PSF Nanocomposite Membranes. Table 1 demonstrates the contact angle values of the pristine PSF membrane and its corresponding composite membranes. The results show that the inclusion of nanoparticles into the composite membranes reduces the water contact angle, and the tendency of water molecules to wet the surface of the PSF membranes increases. A lower contact angle is observed for membranes with Cu_xS-NrGO nanohybrids because of the highly hydrophilic nature of Cu_xS-NrGO (obtained due to nitrogen doping) with the lowest being 59.45° for the 1.5 wt % Cu_xS-NrGO membrane. In addition, CuS-rGO membranes can be considered more hydrophobic than Cu_xS-NrGO membranes because of the rGO sheets, which tend to agglomerate (when there is no heteroatom doping) due to their strong $\pi-\pi$ interactions, and this also

https://doi.org/10.1021/acsomega.1c07140
ACS Omega 2022, 7, 9674−9683

Table 1. Contact Angle Values of the Prepared Pristine and Composite Membranes[a]

membranes	contact angle (°)		
M0	79.65		
	contact angle (°)		
membranes	PSF-CuS	PSF-Cu_xS-NrGO	PSF-CuS-rGO
0.5 wt % NP + PSF	76.85	65.36	73.76
1 wt % NP + PSF	74.32	62.17	70.11
1.5 wt % NP + PSF	71.90	59.45	68.53

[a]NP: nanoparticles.

reduces the specific surface area (17 m^2 g^{-1}). The wettability of the membrane surface increases with an increase in Cu_xS-NrGO nanohybrid incorporation, and the contact angle reduces from 79 to 59°. N doping plays a substantial role in enhancing the hydrophilicity of Cu_xS-NrGO membranes, thus increasing the membrane's affinity to water molecules.

As shown in Figure 7, chemical interactions such as H-bonding and van der Waals are possible between the functional

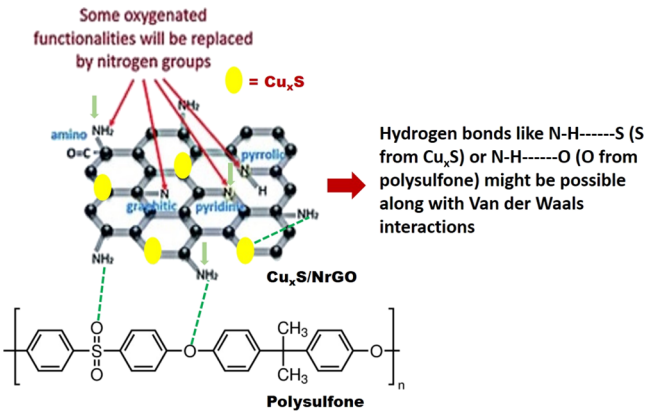

Figure 7. Possible chemical interaction between the synthesized nanohybrids and the polysulfone polymer.

groups of nitrogenated GO and polysulfone membranes making them more compatible with each other. N doping of GO also provides strong interaction with the CuS nanoparticles along with polysulfone, which helps in generating more active sites in the membrane, which in turn enhances the hydrophilicity. Also, the strong interaction between the π electrons of GO and the lone-pair electrons of nitrogen dominantly overcomes the agglomeration leading to better dispersion.

Zeta potential analysis has been performed to determine the surface charge of the prepared membranes. As shown in Table 2, all the prepared PSF membranes are negatively charged; nevertheless, the negative charge increases for PSF-Cu_xS-NrGO membranes with an increase in the loading of Cu_xS-NrGO nanoparticles (0.5−1.5 wt %) into membranes from −19.23 to −46.65 mV. The increase in negative charge distribution on the membrane surface is because of the presence of a higher number of N-active sites, which induces a more negative charge on the PSF membranes. However, the zeta potential values of PSF-CuS and PSF-CuS-rGO membranes are lower than those of PSF-Cu_xS-NrGO membranes. Hence, it can be concluded that the N doping to GO-supported metal nanoparticles helps in drastically improving the surface charge, reducing agglomeration, which can either enhance or repel the feed or the foulant to a very large extent. A higher zeta potential refers to higher stability and less agglomeration, which is observed in the present case and is in good agreement with the literature.[27]

Table 2. Zeta Potential Values of the Prepared Composite Membranes

zeta potential (mV) at pH = 7		
PSF-CuS	PSF-Cu_xS-NrGO	PSF-CuS-rGO
−19.23 (M0)		
−22.15 (M1)	−37.39 (M1CN)	−28.35 (M1Cr)
−25.91 (M2)	−45.90 (M2CN)	−32.75 (M2Cr)
−26.99 (M3)	−46.65 (M3CN)	−37.87 (M3Cr)

Table 3 shows the porosity and mean pore size values of the PSF membrane and its composites. As shown, the porosity and mean pore size of Cu_xS-NrGO membranes are greater than those of pristine PSF and PSF-CuS membranes. The porosity increased from 20.8 to 26.18% and the mean pore size increased from 2.16 to 2.65 nm upon incorporation of Cu_xS-NrGO nanoparticles and increased further with an increase in the loading concentration. This increase is due to the presence of metal nanoparticle-supported nitrogenated GO in the membrane matrix, which facilitates the easy formation of the water layer on the membrane surface because of its stronger affinity toward water molecules, which in turn enhances the porosity and mean pore size of the membranes.

Table 3. Porosities and Mean Pore Sizes of the Prepared Pristine and Composite Membranes

membranes	porosity (%)	mean pore size (nm)
M0	20.8 ± 2.1	2.16 ± 1.6
M1	23.6 ± 1.9	2.25 ± 1.8
M2	26.98 ± 2.5	2.76 ± 0.4
M3	18.4 ± 2.6	1.96 ± 0.9
M1CN	26.43 ± 1.8	2.65 ± 0.9
M2CN	29.18 ± 2.2	3.01 ± 1.2
M3CN	36.85 ± 3.2	3.03 ± 0.6

2.3. Permeation Study. Figure 8 shows the PWF of prepared membranes. The PWF of all the composite membranes increased when compared to the pristine PSF membrane. The results show that the PWF of Cu_xS-NrGO-

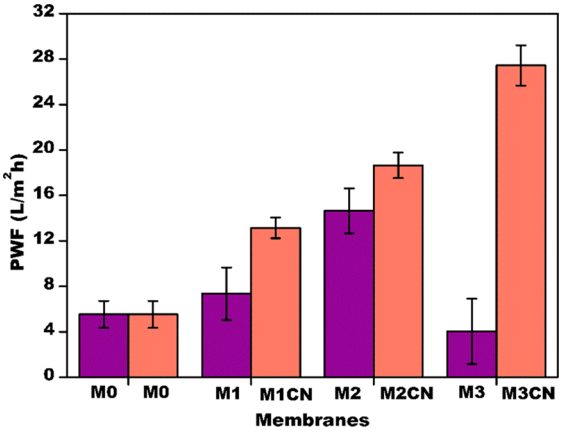

Figure 8. PWF of the pristine PSF membrane and its composites.

https://doi.org/10.1021/acsomega.1c07140
ACS Omega 2022, 7, 9674−9683

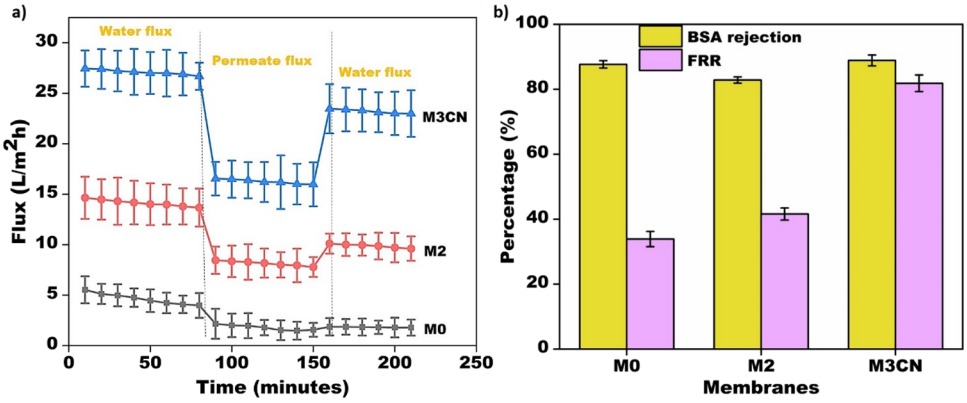

Figure 9. (a) Pure water flux and permeate flux during BSA filtration and (b) percentage of the FRR and BSA rejection of M0, M2, and M3CN membranes.

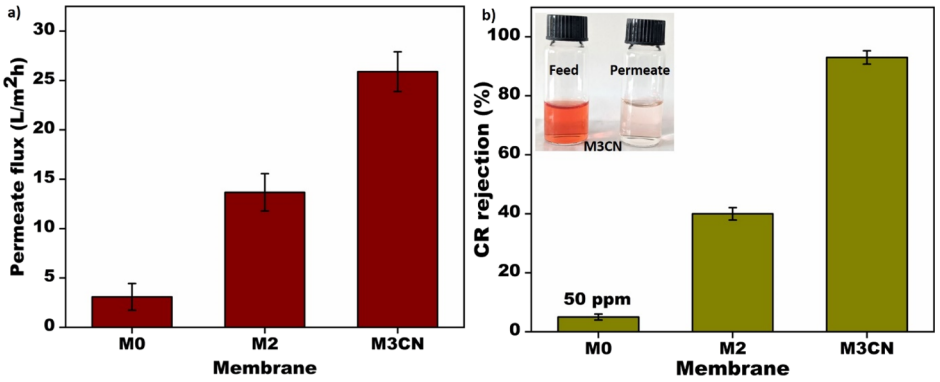

Figure 10. (a) Permeate flux during CR removal and (b) CR rejection % for M0, M2, and M3CN membranes.

incorporated PSF composite membranes was higher than those of CuS-incorporated PSF membranes and CuS-rGO membranes (Table S2) because of the increased hydrophilicity, porosity, and mean pore size of the membranes. Cu_xS-NrGO particles also tend to reduce nanoparticle agglomeration in membranes giving an enhanced pore structure and organized channels for better water diffusion, and this can be well observed in FESEM images. The maximum PWF is observed for the membrane with a 1.5 wt % Cu_xS-NrGO concentration. The hydrophilic nature of Cu_xS-NrGO nanohybrids increases the significant interaction of the membrane with water molecules leading to a higher PWF, and as expected, a higher hydrophilicity and porosity provide better water permeability. The permeability value increases from 14 to 27.43 LMH upon an increase in the loading of Cu_xS-NrGO nanohybrids into the membrane matrix. However, in the case of PSF-CuS membranes, the membrane with 1.5 wt % CuS particles showed a lower flux due to severe agglomeration. The permeability value of PSF-CuS-rGO nanocomposite membranes is given in Table S2 (SI) and is found to be lower than that of Cu_xS-NrGO membranes. In conclusion, Cu_xS-NrGO membranes show almost 30 times better permeation than CuS and CuS-rGO membranes for the highest-concentration nanoparticle-loaded membranes.

2.4. Antifouling Performance of Membranes. Pristine PSF, 1 wt % PSF-CuS, 1.5 wt % Cu_xS-NrGO, and 1.5 wt % CuS-rGO membranes have been chosen for the antifouling study. Figure 9a shows the flux of pure water and BSA solution of the pristine PSF membrane and its composites. The flux of BSA solution for all the membranes was quite lower than the PWF of the same membranes due to pore blockage and cake formation by BSA molecules on the surface of membranes. However, the PWF in the case of the 1.5 wt % Cu_xS-NrGO membrane was restored to a large extent after physical cleaning when compared to pristine PSF and 1 wt % PSF-CuS membranes. The higher PWF restoration rate is due to increased hydrophilicity, which in turn reduces the fouling tendency.

The antifouling performance of the prepared membranes was demonstrated by determining the FRR using BSA protein as a foulant. Figure 9b shows the BSA rejection and the FRR of composite membranes. The 1.5 wt % Cu_xS-NrGO membrane showed a better FRR of nearly 82% as compared to the 1.5 wt % PSF-CuS-rGO, 1 wt % PSF-CuS, and pristine PSF membranes, which showed only 72, 41, and 33%, respectively. The antifouling study of 1.5 wt % PSF-CuS-rGO membranes is shown in the Supporting Information (Figure S6). The excellent antifouling property of the 1.5 wt % Cu_xS-NrGO membrane is because of the presence of hydrophilic Cu_xS-NrGO particles. The formation of an aqueous layer on the surface of the membrane due to increased hydrophilicity repels the adsorption of foulants on the membrane surface. This active layer thus acts as a barrier in controlling the fouling. Along with that, the higher negative zeta potential values prevent the foulant adsorption on the membrane surface (since BSA is also negatively charged), thus eventually increasing the antifouling property of the membranes. Also, no leaching of nanoparticles was observed up to 15 days (determined using AAS).

https://doi.org/10.1021/acsomega.1c07140
ACS Omega 2022, 7, 9674−9683

2.5. Congo Red Dye Removal Studies. Congo red (CR) dye removal studies have been performed with a 50 ppm concentration for the selected optimum pristine PSF (M0), 1 wt % PSF-CuS (M2), and 1.5 wt % Cu_xS-NrGO (M3CN) membranes. From Figure 10, it is clear that the permeate flux (Figure 10a) and congo red dye removal (Figure 10b) are higher for the M3CN membrane than for M0 and M2. The higher permeate flux of 26 L/m^2 h is because of better porosity, and ∼93% rejection of congo red is because of the electrostatic repulsion between the negatively charged dye and the Cu_xS-NrGO membrane as per zeta potential measurements (Table 2).

3. CONCLUSIONS

Cu_xS-NrGO nanoparticles were successfully designed and used for the modification of PSF nanocomposite membranes to improve their antifouling properties. Water contact angle measurements confirm the enhancement in hydrophilicity of these modified membranes after incorporation of Cu_xS-NrGO nanohybrids, thus leading to an improved water permeation flux. An increase in the amount of incorporated Cu_xS-NrGO proportionately enhances the PWF evidencing its nanoparticles in enhancing the PWF. The increase in hydrophilicity and permeability is because of N doping to GO; the N doping helps in increasing the number of N-active sites, which eventually increases the tendency to attract water molecules. Also, the antifouling property of the Cu_xS-NrGO-incorporated PSF membranes enhanced with a flux recovery ratio of ∼80% when compared to bare PSF and PSF-CuS membranes, which showed only 30 and 42% FRR, respectively. A high congo red rejection of ∼93% was also observed for the PSF-Cu_xS-NrGO membrane. Thus, the Cu_xS-NrGO nanohybrids are considerably effective in ameliorating the antifouling property and dye removal capacity of membranes. In situ synthesis helps in increasing the surface area and reduces agglomeration. Doping of GO with nitrogen helps in increasing the interlayer spacing between GO sheets, which in turn increases the surface area, reduces agglomeration, and enhances the conjugated structure. This study hence offers the concept of doping N into rGO to enhance the properties of membranes to almost double their performance in terms of antifouling, rejection, and PWF rates.

4. EXPERIMENTAL SECTION

4.1. Materials. Copper(III) nitrate trihydrate, carbon disulfide, potassium hydroxide, hexadecylamine, *N*-methyl-2-pyrrolidone (NMP), methanol, triethanolamine, potassium permanganate, sodium nitrate, sulfuric acid, and hydrochloric acid were purchased from Merck; polysulfone (P 3500) was from Udel. Bovine serum albumin (BSA) and congo red were from SD Fine Chem Ltd. All other chemicals used were of reagent grade.

4.2. In Situ Synthesis of CuS-NrGO Nanoparticles. Graphene oxide was prepared by the modified Hummers' method.[28] The detailed procedure is given in Supporting Information, Section S1.1 (SI). The synthesis of Cu_xS-NrGO (50/50) was performed as reported in the literature.[18,29] Initially, 0.74 g of aqueous copper nitrate, 0.40 g of potassium hydroxide, 1.4 g of hexadecylamine, and 2 mL of carbon disulfide were placed in 20 mL of methanol solution and stirred for 2 h. To the above solution, 0.5 g of GO was added under stirring for 45 min. This solution was heated to 200 °C for 12 h, and then, the obtained compound was washed with water and ethanol several times to remove traces of impurities left. Finally, the CuS-NrGO nanohybrids were dried in a vacuum oven at 60 °C for 24 h. The procedure for the synthesis of CuS-rGO nanoparticles is given in Section S1.2 (SI).

4.3. Materials Characterization. The morphology of Cu_xS-NrGO nanohybrids was characterized by a field-emission scanning electron microscope supplied by JEOL (JSM 7100F) by spreading the particles on carbon tape with a gold coating of 20 nm. Transmission electron microscopy (TEM) studies were carried out using a TALOS F200S G2 with a 200 kV accelerating voltage by dispersing the nanoparticles in ethanol, and then, the dilute solution was drop cast on a Cu grid. EDX analysis was performed to analyze the dispersion of Cu_xS nanoparticles on NrGO sheets. Elemental analysis was performed using an X-ray photoelectron spectrometer (XPS) equipped with Al Kα (1486.6 eV) as the X-ray source and a pass energy of 50 eV. The crystal structure was analyzed by powder XRD using Cu Kβ radiation (Rigaku (Japan)) at a scan rate of 3° min^{-1} operated at 40 kV from 5 to 80°. The average crystallite size (D) was estimated using the Scherrer equation (eq 1) as mentioned below:[2]

$$D = \frac{0.9\lambda}{\beta \cos\theta} \quad (1)$$

where λ is the X-ray wavelength and β is the full width at half-maximum of the intensity peak at the corresponding Bragg's diffraction angle (θ).

4.4. Preparation of Cu_xS-NrGO Nanohybrid-Incorporated Polysulfone MMMs. The nanohybrid-incorporated polysulfone mixed matrix membranes were prepared by a diffusion-induced phase separation (DIPS) method as reported in the literature.[30] Initially, the calculated amounts of Cu_xS-NrGO nanohybrids (as shown in Table 4) were dispersed in NMP solution using an ultrasonicator for 2 h; then, suitable amounts of PSF were added with continuous stirring at 45 °C. The stirring was continued until a homogeneous solution was obtained. The obtained casting solution was kept aside for a few minutes to remove air bubbles. It was then cast on a clean glass plate using a casting knife and immersed in a coagulation bath containing distilled water wherein the phase inversion took place. After 24 h, the membrane was peeled off from the glass plate and washed thoroughly with distilled water to remove traces of the solvent left. The washed membranes were then stored in distilled water until further use. The same procedure was followed for the fabrication of membranes with

Table 4. Compositions of PSF Membranes with Different Concentrations of CuS and Cu_xS-NrGO Nanohybrids[a]

	composition (wt %)			
membrane	PSF	CuS	Cu_xS-NrGO	NMP
M0	17	0	0	83
M1	16.5	0.5	0	83
M2	16	1.0	0	83
M3	15.5	1.5	0	83
M1CN	16.5	0	0.5	83
M2CN	16	0	1.0	83
M3CN	15.5	0	1.5	83

[a]Note: More agglomeration was observed when the concentration was beyond 1.5 wt % CuS-NrGO. Hence, the studies were restricted to 1.5 wt % CuS-NrGO.

https://doi.org/10.1021/acsomega.1c07140
ACS Omega 2022, 7, 9674−9683

CuS and CuS-rGO nanoparticles. Compositions of CuS-rGO-incorporated PSF membranes are given in the SI (Table S1).

4.5. Membrane Characterization. XRD patterns were obtained for prepared MMMs using a powder X-ray diffractometer (Rigaku, Japan) equipped with a nickel-filtered Cu Kβ radiation source. EDX elemental mapping was also done to confirm the successful embedment of nanohybrids into MMMs. The cross-sectional images of the modified PSF membranes were captured using a JSM 7100F JEOL FESEM with an accelerating voltage of 5 kV. To quantify the hydrophilicity of the prepared PSF-based membranes, measurements of the static contact angle based on the sessile drop method were carried out using a contact angle meter (KYOWA, Japan). To determine the surface charge of the membranes, zeta potential analysis was carried out.[31] A detailed explanation is given in the Supporting Information (Sections S2.1−S2.3).

4.6. Membrane Performance. The pure water flux of the prepared membranes was measured using a self-constructed dead-end filtration unit.[32] Performance evaluation of nanohybrid-functionalized PSF MMMs was done via antifouling studies and dye removal capacity. BSA was used as a foulant to study the rejection capacity of prepared membranes.[7] Antifouling properties of the prepared membranes were determined using a dead-end filtration unit, and BSA of 200 mgL^{-1} concentration was used as a foulant.[7,33] Congo red with a 50 ppm concentration was chosen to study the dye removal capacity of the membranes. The detailed procedure of all the performance studies is given in the Supporting Information (Sections S3.1−S3.4).

■ ASSOCIATED CONTENT

Supporting Information

The Supporting Information is available free of charge at https://pubs.acs.org/doi/10.1021/acsomega.1c07140.

GO and CuS-rGO synthesis procedures (Sections S1.1 and S1.2); characterization procedures of FESEM, contact angle, and zeta potential measurements (Sections S2.1−S2.3); procedures for PWF, BSA filtration, antifouling, and dye removal studies (Sections S3.1−S3.4); XRD spectrum, FESEM images, TEM images, and EDX spectra of CuS-rGO nanoparticles (Sections S4.1−S4.3); XRD spectra and permeability studies of bare PSF and PSF-CuS-rGO membranes (Sections S4.4 and S4.5) (PDF)

■ AUTHOR INFORMATION

Corresponding Authors

R Geetha Balakrishna − *Centre for Nano and Materials Sciences, Jain University, Jain Global Campus, Bangalore 562112, India;* orcid.org/0000-0002-7247-4921; Email: br.geetha@jainuniversity.ac.in

Farid A. Harraz − *Promising Centre for Sensors and Electronic Devices (PCSED), Advanced Materials and Nano-Research Centre, Najran University, Najran 11001, Saudi Arabia; Nanomaterials and Nanotechnology Department, Central Metallurgical Research and Development Institute (CMRDI), Cairo 11421, Egypt;* orcid.org/0000-0001-7776-7099; Email: faharraz@nu.edu.sa

Authors

Lavanya Chandra − *Centre for Nano and Materials Sciences, Jain University, Jain Global Campus, Bangalore 562112, India*

Kusuma Jagadish − *Centre for Nano and Materials Sciences, Jain University, Jain Global Campus, Bangalore 562112, India*

Vinothkumar Karthikeyarajan − *Centre for Nano and Materials Sciences, Jain University, Jain Global Campus, Bangalore 562112, India*

Mohammed Jalalah − *Promising Centre for Sensors and Electronic Devices (PCSED), Advanced Materials and Nano-Research Centre and Department of Electrical Engineering, Faculty of Engineering, Najran University, Najran 11001, Saudi Arabia*

Mabkhoot Alsaiari − *Promising Centre for Sensors and Electronic Devices (PCSED), Advanced Materials and Nano-Research Centre and Department of Chemistry, Faculty of Science and Arts at Sharurah, Najran University, Najran 11001, Saudi Arabia;* orcid.org/0000-0002-4366-3256

Complete contact information is available at: https://pubs.acs.org/10.1021/acsomega.1c07140

Notes

The authors declare no competing financial interest.

■ ACKNOWLEDGMENTS

The authors would like to acknowledge the Deputy for Research and Innovation−Ministry of Education, Kingdom of Saudi Arabia for this research through a grant (NU/IFC/INT/01/002) under the institutional funding committee at Najran University, Kingdom of Saudi Arabia and the support from the Naval Research Board (NRB/4003/PG/363), Govt of India.

■ REFERENCES

(1) (a) Ng, L. Y.; Mohammad, A. W.; Leo, C. P.; Hilal, N. Polymeric membranes incorporated with metal/metal oxide nanoparticles: A comprehensive review. *Desalination* **2013**, *308*, 15−33. (b) Zahid, M.; Rashid, A.; Akram, S.; Rehan, Z. A.; Razzaq, W. A Comprehensive Review on Polymeric Nano-Composite Membranes for Water Treatment. *J. Membr. Sci. Technol.* **2018**, *08*, 1.

(2) Saranya, R.; Arthanareeswaran, G.; Ismail, A. F.; Reddy, N. L.; Shankar, M. V.; Kweon, J. Efficient rejection of organic compounds using functionalized ZSM-5 incorporated PPSU mixed matrix membrane. *RSC Adv.* **2017**, *7*, 15536−15552.

(3) Zularisam, A. W.; Ismail, A. F.; Salim, M. R.; Sakinah, M.; Hiroaki, O. Fabrication, fouling and foulant analyses of asymmetric polysulfone (PSF) ultrafiltration membrane fouled with natural organic matter (NOM) source waters. *J. Membr. Sci.* **2007**, *299*, 97−113.

(4) Zhang, R.; Liu, Y.; He, M.; Su, Y.; Zhao, X.; Elimelech, M.; Jiang, Z. Antifouling membranes for sustainable water purification: strategies and mechanisms. *Chem. Soc. Rev.* **2016**, *45*, 5888−5924.

(5) Lee, A.; Elam, J. W.; Darling, S. B. Membrane materials for water purification: design, development, and application. *Environ. Sci. Water Res. Technol.* **2016**, *2*, 17−42.

(6) Mokhtari, S.; Rahimpour, A.; Shamsabadi, A. A.; Habibzadeh, S.; Soroush, M. Enhancing performance and surface antifouling properties of polysulfone ultrafiltration membranes with salicylate-alumoxane nanoparticles. *Appl. Surf. Sci.* **2017**, *393*, 93−102.

(7) Khorshidi, B.; Hosseini, S. A.; Ma, G.; McGregor, M.; Sadrzadeh, M. Novel nanocomposite polyethersulfone- antimony tin oxide membrane with enhanced thermal, electrical and antifouling properties. *Polymer* **2019**, *163*, 48−56.

(8) Maximous, N.; Nakhla, G.; Wan, W.; Wong, K. Effect of the metal oxide particle distributions on modified PES membranes characteristics and performance. *J. Membr. Sci.* **2010**, *361*, 213−222.
(9) Kuvarega, A. T.; Khumalo, N.; Dlamini, D.; Mamba, B. B. Polysulfone/N,Pd co-doped TiO2 composite membranes for photocatalytic dye degradation. *Sep. Purif. Technol.* **2018**, *191*, 122−133.
(10) Tabish, T. A.; Memon, F. A.; Gomez, D. E.; Horsell, D. W.; Zhang, S. A facile synthesis of porous graphene for efficient water and wastewater treatment. *Sci. Rep.* **2018**, *8*, 1817.
(11) Zhang, X.; Liu, Y.; Sun, C.; Ji, H.; Zhao, W.; Sun, S.; Zhao, C. Graphene oxide-based polymeric membranes for broad water pollutant removal. *RSC Adv.* **2015**, *5*, 100651−100662.
(12) Pei, J.; Zhang, X.; Huang, L.; Jiang, H.; Hu, X. Fabrication of reduced graphene oxide membranes for highly efficient water desalination. *RSC Adv.* **2016**, *6*, 101948−101952.
(13) Wang, X.; Sun, G.; Routh, P.; Kim, D. H.; Huang, W.; Chen, P. Heteroatom-doped graphene materials: syntheses, properties and applications. *Chem. Soc. Rev.* **2014**, *43*, 7067−7098.
(14) Liu, Y.; Yu, L.; Ong, C. N.; Xie, J. Nitrogen-doped graphene nanosheets as reactive water purification membranes. *Nano Res.* **2016**, *9*, 1983−1993.
(15) (a) Nolan, H.; Mendoza-Sanchez, B.; Ashok Kumar, N.; McEvoy, N.; O'Brien, S.; Nicolosi, V.; Duesberg, G. S. Nitrogen-doped reduced graphene oxide electrodes for electrochemical supercapacitors. *Phys. Chem. Chem. Phys.* **2014**, *16*, 2280−2284. (b) Xing, Z.; Ju, Z.; Zhao, Y.; Wan, J.; Zhu, Y.; Qiang, Y.; Qian, Y. One-pot hydrothermal synthesis of Nitrogen-doped graphene as high-performance anode materials for lithium ion batteries. *Sci. Rep.* **2016**, *6*, 26146.
(16) Bag, S.; Raj, C. R. On the electrocatalytic activity of nitrogen-doped reduced graphene Oxide: Does the nature of nitrogen really control the activity towards oxygen reduction? *J. Chem. Sci.* **2016**, *128*, 339−347.
(17) (a) Kumar, K. V.; Preuss, K.; Guo, Z. X.; Titirici, M. M. Understanding the Hydrophilicity and Water Adsorption Behavior of Nanoporous Nitrogen-Doped Carbons. *J. Phys. Chem. C* **2016**, *120*, 18167−18179. (b) Sun, H.; Wang, Y.; Liu, S.; Ge, L.; Wang, L.; Zhu, Z.; Wang, S. Facile synthesis of nitrogen doped reduced graphene oxide as a superior metal-free catalyst for oxidation. *Chem. Commun.* **2013**, *49*, 9914−9916. (c) Wang, H.; Maiyalagan, T.; Wang, X. Review on Recent Progress in Nitrogen-Doped Graphene: Synthesis, Characterization, and Its Potential Applications. *ACS Catal.* **2012**, *2*, 781−794. (d) Mageed, A. K.; AB, D. R.; Salmiaton, A.; Izhar, S.; Razak, M. A.; Yusoff, H.; Yasin, F.; Kamrudin, S. Preparation and characterization of nitrogen doped reduced graphene oxide sheet. *Int. J. Appl. Chem.* **2016**, *12*, 104−108.
(18) Giribabu, K.; Oh, S. Y.; Suresh, R.; Kumar, S. P.; Manigandan, R.; Munusamy, S.; Gnanamoorthy, G.; Kim, J. Y.; Huh, Y. S.; Narayanan, V. Sensing of picric acid with a glassy carbon electrode modified with CuS nanoparticles deposited on nitrogen-doped reduced graphene oxide. *Microchim. Acta* **2016**, *183*, 2421−2430.
(19) (a) Guo, J.; Huo, J.; Liu, Y.; Wu, W.; Wang, Y.; Wu, M.; Liu, H.; Wang, G. Nitrogen-Doped Porous Carbon Supported Nonprecious Metal Single-Atom Electrocatalysts: from Synthesis to Application. *Small Methods* **2019**, *3*, 1900159. (b) Naderi, H. R.; Sobhani-Nasab, A.; Rahimi-Nasrabadi, M.; Ganjali, M. R. Decoration of nitrogen-doped reduced graphene oxide with cobalt tungstate nanoparticles for use in high-performance supercapacitors. *Appl. Surf. Sci.* **2017**, *423*, 1025−1034.
(20) Sanka, R. V. S. P.; Balaji, K.; Leterrier, Y.; Pandey, S.; Srivastava, M.; Srivastava, A.; Binder, W. H.; Rana, S.; Michaud, V. Nitrogen-doped graphene stabilized copper nanoparticles for Huisgen [3+2] cycloaddition "click" chemistry. *Chem. Commun.* **2019**, *55*, 6249−6252.
(21) Horikawa, T.; Sakao, N.; Hayashi, J.'i.; Do, D. D.; Katoh, M.; Sotowa, K. I. Preparation of nitrogen-doped poros carbon and its water adsorption properties. *Adsorpt. Sci. Technol.* **2012**, *31*, 135−144.
(22) (a) Yuan, D.; Huang, G.; Zhang, F.; Yin, D.; Wang, L. Facile synthesis of CuS/rGO composite with enhanced electrochemical lithium-storage properties through microwave-assisted hydrothermal method. *Electrochim. Acta* **2016**, *203*, 238−245. (b) Yuan, B.; Gao, Q.; Zhang, X.; Duan, L.; Chen, L.; Mao, Z.; Li, X.; Lü, W. Reduced graphene oxide (RGO)/Cu2S composite as catalytic counter electrode for quantum dot-sensitized solar cells. *Electrochim. Acta* **2018**, *277*, 50−58.
(23) (a) Hu, X.-S.; Shen, Y.; Zhang, Y.-T.; Zhang, H.-F.; Xu, L.-H.; Xing, Y.-J. Synthesis of flower-like CuS/reduced graphene oxide (RGO) composites with significantly enhanced photocatalytic performance. *J. Alloys Compd.* **2017**, *695*, 1778−1785. (b) Liu, H. Flower-like CuS/reduced Graphene Oxide Composite as Anode Materials for Lithium Ion Batteries. *Int. J. Electrochem. Sci.* **2018**, *13*, 4775−4781. (c) Bai, J.; Jiang, X. A facile one-pot synthesis of copper sulfide-decorated reduced graphene oxide composites for enhanced detecting of H2O2 in biological environments. *Anal. Chem.* **2013**, *85*, 8095−8101. (d) Modi, A.; Bellare, J. Copper sulfide nanoparticles/carboxylated graphene oxide nanosheets blended polyethersulfone hollow fiber membranes: Development and characterization for efficient separation of oxybenzone and bisphenol A from water. *Polymer* **2019**, *163*, 57−67.
(24) Jain, M.; Babar, D. G.; Garje, S. S. Ligand-based stoichiometric tuning in copper sulfide nanostructures and their catalytic ability. *Appl. Nanosci.* **2019**, *9*, 353−367.
(25) Boytsov, O.; Ustinov, A. I.; Gaffet, E.; Bernard, F. Correlation between milling parameters and microstructure characteristics of nanocrystalline copper powder prepared via a high energy planetary ball mill. *J. Alloys Compd.* **2007**, *432*, 103−110.
(26) AlShammari, A. S.; Halim, M. M.; Yam, F. K.; Kaus, N. H. M. Effect of precursor concentration on the performance of UV photodetector using TiO2/reduced graphene oxide (rGO) nanocomposite. *Results Phys.* **2020**, *19*, 103630.
(27) (a) Gao, G. W. L. a. P. Emulsions and microemulsions for topical and transdermal drug delivery. In *Handbook of non-invasive drug delivery systems*; William Andrew Applied Science Publishers: 2010, pp. 59−64; (b) Samimi, S.; Maghsoudnia, N.; Eftekhari, R. B.; Dorkoosh, F. Lipid-Based Nanoparticles for Drug Delivery Systems. In *Characterization and Biology of Nanomaterials for Drug Delivery*; 2019, pp. 47−76, DOI: 10.1016/B978-0-12-814031-4.00003-9.
(28) Chen, J.; Yao, B.; Li, C.; Shi, G. An improved Hummers method for eco-friendly synthesis of graphene oxide. *Carbon* **2013**, *64*, 225−229.
(29) Kong, C.; Min, S.; Lu, G. Dye-Sensitized NiS_x Catalyst Decorated on Graphene for Highly Efficient Reduction of Water to Hydrogen under Visible Light Irradiation. *ACS Catal.* **2014**, *4*, 2763−2769.
(30) Lavanya, C.; Geetha Balakrishna, R. Naturally derived polysaccharides-modified PSF membranes: A potency in enriching the antifouling nature of membranes. *Sep. Purif. Technol.* **2020**, *230*, 115887.
(31) Lavanya, C.; Kusuma, J.; Geetha Balakrishna, R. Pyrochlores: oxygen-rich moieties as ceramic fillers in uplifting the antifouling property and dye removal capacity of polymeric membranes. *Sep. Purif. Technol.* **2021**, *272*, 118946.
(32) Lavanya, C.; Balakrishna, R. G.; Soontarapa, K.; Padaki, M. S. Fouling resistant functional blend membrane for removal of organic matter and heavy metal ions. *J. Environ. Manage.* **2019**, *232*, 372−381.
(33) Lavanya, C.; Soontarapa, K.; Jyothi, M. S.; Balakrishna, R. G. Environmental friendly and cost effective caramel for congo red removal, high flux and fouling resistance of polysulfone membranes. *Sep. Purif. Technol.* **2019**, *211*, 348−358.

https://doi.org/10.1021/acsomega.1c07140
ACS Omega 2022, 7, 9674−9683